Flexural stresses beneath Hawaii: Implications for the October 15, 2006, earthquakes and magma ascent

Patrick J. McGovern[1]

Received 12 July 2007; revised 18 September 2007; accepted 15 October 2007; published 8 December 2007.

[1] On October 15, 2006, two large earthquakes rocked the northwest coast of the island of Hawaii six minutes apart: the Kiholo Bay and Mahukona events, with magnitudes M_w = 6.7 and 6.0, respectively. Their close proximity in space and time suggests a common origin, but sharp contrasts in mechanism and depth present an unusual fault-aftershock relationship. Here I account for the October 15th earthquakes as the divergent outcomes of a single process: downward flexing of the lithosphere in response to loading by Hawaiian volcanoes. Viscoelastic finite element models of lithospheric flexure reveal that a strong stiffness contrast between crustal and mantle materials produces peak upper lithosphere stresses at the top of the stiffer mantle. High compression at the mantle top explains the tendency to trap magmas near the base of the crust: the underplating observed seismically at older Hawaiian volcanoes. These phenomena produce peak stress regions at depths consistent with that of the unexpectedly deep Mahukona event. **Citation:** McGovern, P. J. (2007), Flexural stresses beneath Hawaii: Implications for the October 15, 2006, earthquakes and magma ascent, *Geophys. Res. Lett.*, *34*, L23305, doi:10.1029/2007GL031305.

1. Introduction

[2] The Hawaiian earthquake sequence of October 15th 2006 comprised two events with magnitudes $M_w > 6$ (Figure 1) and several smaller aftershocks. The initial event, Kiholo Bay, occurred at 7:07 AM local time at a depth of 39 km [*Nakata*, 2007], with teleseismically determined magnitude M_w = 6.7 and a focal mechanism consistent with oblique normal faulting (Global CMT catalog, available at http://www.globalcmt.org, 2007). About six minutes later the Mahukona event struck at a depth of 19 km [*Nakata*, 2007], with M_w = 6.0 and a compressional focal mechanism (Global CMT catalog, available at http://www.globalcmt.org, 2007). The epicenters were located about 28 km apart (Figure 1). The initial shock caused significant damage along the Hawaiian chain, all the way up to Oahu [*Gramling*, 2007].

[3] The depths of the two major events place them in the mantle. Mantle earthquakes around Hawaii have been attributed to flexural stresses induced by volcanic loading [e.g., *Pritchard et al.*, 2007], although magma-related processes also contribute, especially in shallower regions [*Klein et al.*, 1987; *Wolfe et al.*, 2003]. Most mantle earthquakes are located beneath the southeast portion of the island and are associated with the growth of the younger Mauna Loa and Kilauea edifices [*Wolfe et al.*, 2003; *Pritchard et al.*, 2007]. However, deep large-magnitude earthquakes have also occurred elsewhere, including the 1973 M = 6.2 Honomu event beneath Mauna Kea and an event far to the west of Mauna Loa [*Wolfe et al.*, 2004]. The Honomu, Kiholo Bay, and Mahukona earthquakes suggest that the older Mauna Kea, Hualalai, and Kohala volcanoes (Figure 1) remain capable of inducing high-magnitude stresses in the lithosphere.

[4] The structure of the crust and lithosphere beneath the Hawaiian chain has been constrained by seismic, gravity, and bathymetry data, in conjunction with idealized elastic models of lithospheric flexure. The pre-volcano oceanic crust has an essentially constant thickness of about 6 km [*Hill and Zucca*, 1987]. Determinations of depths to subsurface seismic interfaces and seismic velocity structure indicate that the crust directly beneath the older Hawaiian edifices is thickened by ascending basaltic magma emplaced at the base of the crust [*ten Brink and Brocher*, 1987; *Watts and ten Brink*, 1989], a phenomenon termed "underplating". Flexural models constrained by seismically determined structures yield estimates of the thickness of an idealized elastic plate (the "elastic thickness" T_e) that best fits the data range from 25 to 40 km [*Watts and ten Brink*, 1989; *Wessel*, 1993]. The latter study also considered a more realistic stress vs. depth profile, yielding estimates of the overall mechanical thickness of the lithosphere supporting Hawaii in the range 33–44 km. These models and thickness values have two important implications: First, the lithosphere beneath Hawaii has both crustal and mantle components. Second, the depth of the Mahukona event places it in what is predicted to be a relatively low-stress region of the lithosphere (near the neutral plane of flexure), contrary to the expectation that such earthquakes would occur where stresses are highest: at shallower depths, near the top of the lithosphere.

[5] The cause of crustal underplating is a matter of debate. *ten Brink and Brocher* [1987] invoked interplay between flexural stresses and pressure in a fluid magma column to explain why magma stalls at the base of the crust beneath Hawaii. In this view, ascending magma experienced increasing horizontal compression, impeding ascent via vertical fractures and encouraging formation of horizontal ones. Such a stress state, characteristic of concave-upward flexure, has been invoked as a barrier to magma ascent [e.g., *McGovern and Solomon*, 1993, 1998; *Hieronymus and Bercovici*, 2001; *Pritchard et al.*, 2007]. Stress control also explains the lack of observed underplating beneath the youngest volcanoes of the chain, for which flexural response is incomplete. An alternative view, expressed by *Klügel et al.* [2005] in the context of the Canary Islands, is

[1]Lunar and Planetary Institute, Universities Space Research Association, Houston, Texas, USA.

0094-8276/07/2007GL031305

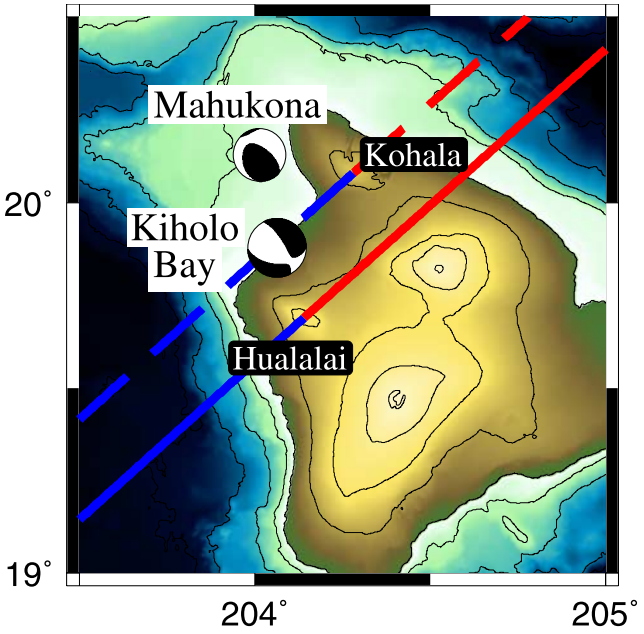

Figure 1. Topographic map of Island of Hawaii [*Eakins et al.*, 2003], with epicenters [*Nakata*, 2007] and focal mechanisms (Global CMT catalog, available at http://www.globalcmt.org, 2007) of Oct. 15, 2006, earthquakes, and cross-section tracks perpendicular to the Hawaiian ridge emanating from the Hualalai and Kohala edifices.

that buoyancy forces control underplating. Ascending magma reaches a zone of neutral buoyancy at the crust-mantle boundary where the driving forces for ascent diminish, resulting in enhanced magma emplacement.

2. Method

[6] I use the TEKTON finite element code [*Melosh and Raefsky*, 1983] to calculate stresses and deformation of a viscoelastic lithosphere with depth-varying properties, subject to loading by Hawaiian volcanoes. TEKTON has a long record of solving tectonic and volcanic loading problems [e.g., *McGovern and Solomon*, 1993, 1998]. The grid extends 1040 km horizontally and 240 km vertically, with best resolution of 2 km by 1 km in the vicinity of the volcanic load. The uppermost layers represent crust and mantle lithosphere; the asthenospheric mantle is assigned a constant Newtonian viscosity, such that the loading timescale is dictated by the characteristic relaxation time of the asthenosphere. Symmetry is assumed along the $x = 0$ vertical axis, such that the model load represents half of the volcanic ridge. All horizontal motions at the left and right boundaries are fixed to zero, as are all vertical motions of the bottom boundary. Material properties for the models are given in Table 1.

[7] Most mantle-depth earthquakes have occurred in the southeast of the island and are associated with the growth of the younger Mauna Loa and Kilauea edifices. However, the northwest corner of Hawaii is dominated by the older Hualalai and Kohala volcanoes (Figure 1): models for the driving stresses for the October 15 earthquakes should therefore conform to their dimensions. Further, the earthquake locations place them in a region where the flexure will be affected by the ridge-like nature of islands farther up the chain. For this reason, I adopt 2-dimensional plane-strain model geometry, a natural choice for ridge structures; load dimensions correspond to topographic cross-sections perpendicular to the ridge (Figure 1). This choice of geometry is further justified by the elongated nature of the flexural response to the whole Hawaiian volcanic chain [e.g., *Pritchard et al.*, 2007, Figure 4c]. The load is represented by point forces applied to the top surface of the lithosphere, representing a ridge of height 14 km and half-width 130 km, but with an embedded high-density dunite cumulate core [e.g., *Clague and Denlinger*, 1994] of height 5 km and half-width 10 km. Ocean-related buoyancy effects are accounted for by reducing the load magnitudes appropriately.

[8] All models have pre-volcano crust and mantle components with appropriate thicknesses and densities. The "uniform elastic plate" model (model "A") has uniform stiffness (Young's Modulus E) and elastic thickness T_e = 30 km. For the "uniform viscoelastic plate" model ("B"), the depth-dependence of lithospheric viscosity is calculated using a linear temperature profile (geotherm) that increases by 17.8° K per km of depth, and rheological constants appropriate to wet olivine [*Karato et al.*, 1986] in the mantle, such that the mechanical thickness of the plate (i.e., the region with finite differential stresses) is about 40 km. For the "viscoelastic layered stiffness" plate (model "C"), the same geotherm is used, but the crust and mantle assume different stiffnesses for crust (basalt) and mantle (dunite) rocks [*Turcotte and Schubert*, 2002]. Material failure is predicted using a Mohr-Coulomb criterion.

[9] Modeling crustal underplating requires consideration of several effects. Assuming this material is emplaced as laterally propagating sills, it would mechanically detach the upper and lower parts of lithosphere. Also, on solidification the initial stress state would be lithostatic, with differential stress accruing only as a result of subsequent loading and/or flexure, thus yielding reduced differential stresses relative to the surrounding lithosphere [e.g., *McGovern and Solomon*, 1993, 1998]. To account for these effects (models "D1" and "D2"), I assign crustal densities and some multiple of

Table 1. Material Properties for Finite Element Models

Property	Value	Model
Crustal thickness T_c	6 km	All
Crustal density	2800 kg/m^3	All
Mantle density	3300 kg/m^3	All
Edifice density	2700 kg/m^3	All
Cumulate density	3100 kg/m^3	All
Young's modulus (uniform)	1.0×10^{11} Pa	A, B
Crustal Young's modulus (layered)	6×10^{10} Pa	C, D
Mantle Young's modulus (layered)	1.6×10^{11} Pa	C, D
Mohr-Coulomb internal friction phi	30°	All
Mohr-Coulomb cohesion	3.5×10^7 Pa	All
Mantle asthenosphere viscosity	1×10^{21} Pa s	All, and underplate for D

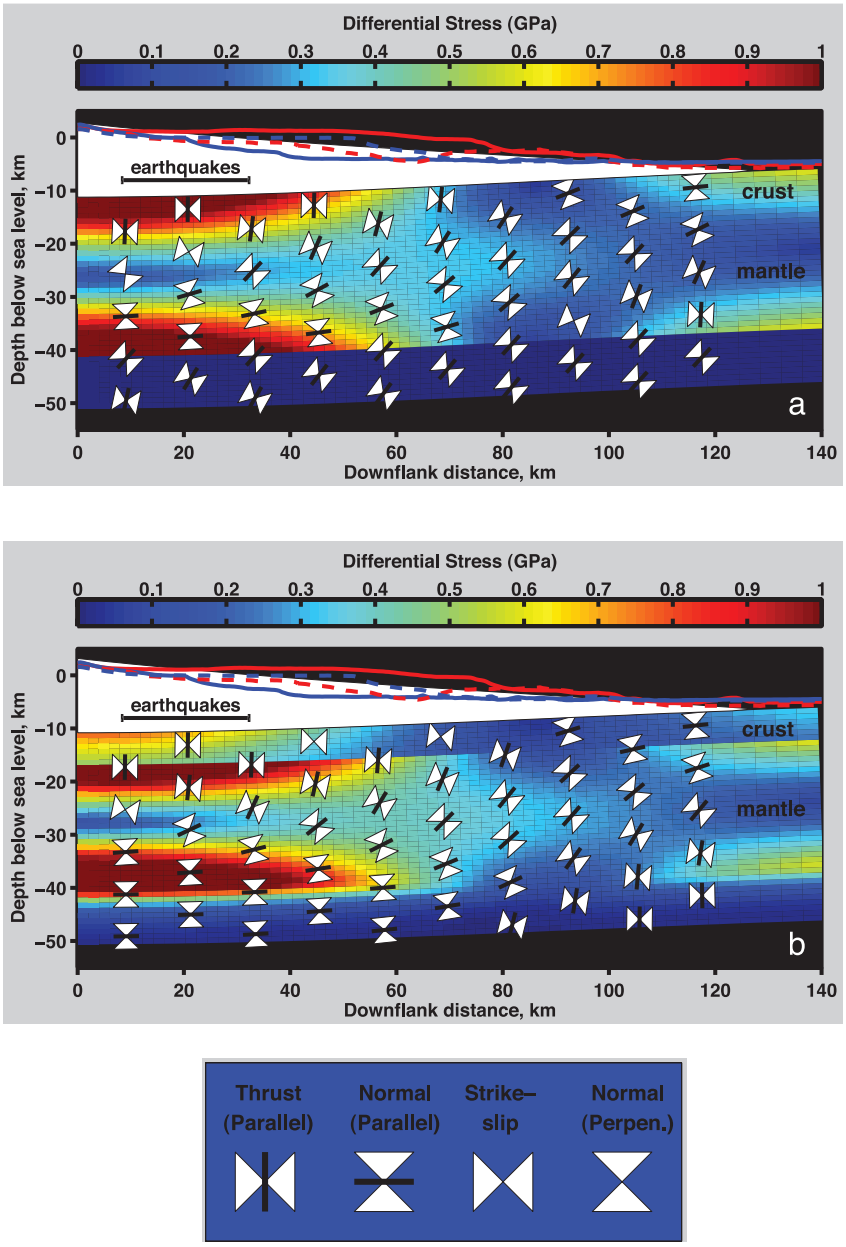

Figure 2. Differential stress magnitudes and principal stress orientations for finite element models of lithospheric flexure. The white wedge-shaped region atop lithosphere delineates the modeled load; blue and red lines denote topography corresponding to cross-sections of Hualalai (solid) and Kohala (dashed) shown in Figure 1. The projected lateral range of the October 15th earthquakes is shown by the black bar. The hourglass-shaped symbols are aligned in the direction of principal compression, bar symbols in directions of principal extension, and an absent bar indicates out-of-plane principal extension. The key at bottom gives examples of the types and orientations (either parallel or perpendicular to the volcanic ridge) of faulting predicted by certain configurations of the stress symbols. (a) Elastic plate with uniform Young's modulus (model A). (b) Viscoelastic plate with stiffness contrast (model C).

asthenospheric viscosities (Table 1) to elements just beneath the base of the crust. Although constraints far from Oahu are limited, *Watts and ten Brink* [1989] infer a limited amount of underplating at the positions of Hualalai and Kohala [*Watts and ten Brink*, 1989, Figure 15]. Thus, I scale the thickness and width of the altered zone to about half of the peak size of the underplated regions beneath Oahu, yielding 2 km height and 80 km half-width, to reflect the early stage of the process at northwest Hawaii.

3. Results

[10] Deformation of and stress state in the lithosphere are shown in Figure 2. The uniform stiffness elastic model "A" (Figure 2a) shows strong differential stress maximums in the upper and lower lithospheres beneath the center of the

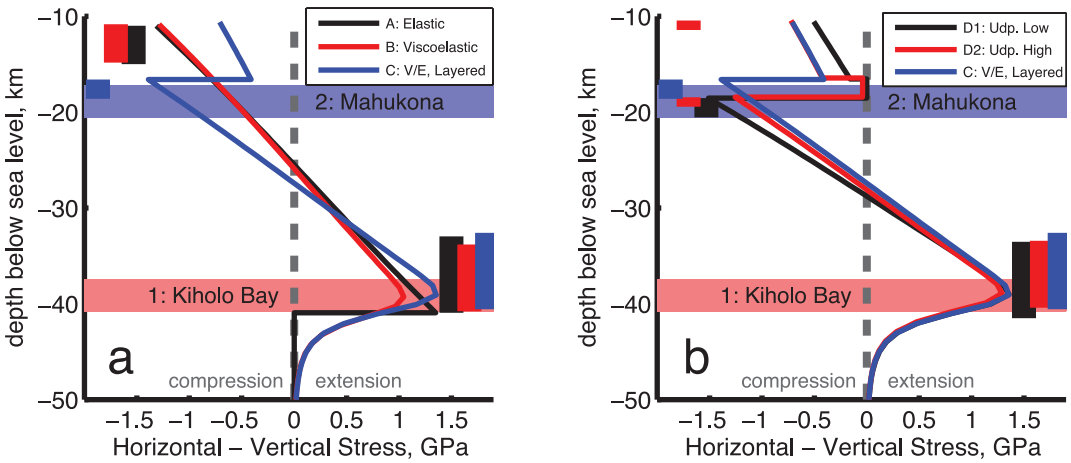

Figure 3. Difference between in-plane horizontal and vertical normal stress vs. depth beneath sea level at a distance 20 km from the load center, for 3 models of flexure. (a) Model A: elastic lithosphere of 30 km thickness, uniform elastic properties (black curve). Model B: viscoelastic lithosphere (ductile flow in lower lithosphere), uniform elastic properties (red curve). Model C: viscoelastic lithosphere with stiffness contrast between crust and mantle (blue curve). Vertical ranges of predicted faulting, calculated via a Mohr-Coulomb failure criterion, are shown by bars (color-coded to the curves) on either side of curves. (b) As in Figure 3a, for models with underplating. Model D1 (black curve), underplating with asthenospheric viscosity. Model D2 (red curve), underplating with 100 × asthenospheric viscosity. Model C (blue curve), same as in Figure 3a.

edifice load (*x*-axis origin), extending laterally to about 50 km or so. Principal stress orientations near this axis indicate horizontal compression in the upper lithosphere and horizontal extension in the lower lithosphere. In a layered-stiffness viscoelastic model (“C”; Figure 2b) the stress state is broadly similar to that of Figure 2a, with two important differences. First, the highest differential stresses in the upper lithosphere are displaced from the top of the crust (i.e., top of the lithosphere) to the top of the mantle (within the lithosphere). Second, a greatly reduced (in both magnitude and areal extent) high-stress region now occurs at the top of the crust (Figure 2b).

[11] To yield insights into the stresses associated with lithospheric earthquakes, we take vertical cross-sections of stress differences in the model lithospheres, at a downflank distance (20 km) that represents an average location of the October 15th earthquakes with respect to the volcanoes. The simplest model, a uniform elastic plate (model “A”) assumes a constant Young’s modulus [e.g., *Pritchard et al.*, 2007] and predicts an extensional stress maximum at the bottom of the lithosphere (black curve in Figure 3a), consistent with the mechanism (extensional) and depth of the Kiholo Bay earthquake. In such models, stress differences by definition drop abruptly from the peak value to zero immediately beneath the plate. However, ductile flow in the warm lower lithosphere will tend to produce an extensional stress peak within the lithosphere rather than at its base. Models with viscoelastic rheology and temperature-dependent viscosity (but maintaining constant Young’s modulus: model “B”) produce such a stress peak (red line in Figure 3), the position of which can be matched to the depth of earthquakes like Kiholo Bay; models with higher or lower thermal gradients have shallower or deeper stress peaks, respectively. In the mid-lithosphere, the stress state for models A and B are very similar. In the upper lithosphere, high compressive stresses are predicted at the top surface of uniform-stiffness plates (black and red lines in Figure 3a). This result is consistent with the mechanism of the Mahukona earthquake (compressional), but not its depth, which places it in the relatively low-stress interior of a uniform-stiffness plate (Figure 3a).

[12] In contrast, models that include significantly greater stiffness for mantle than for crust (e.g., model “C”) produce a sharply defined stress maximum in compression at the top of the mantle lithosphere (blue curve in Figure 3a). Stresses in the crust above are greatly reduced compared to the uniform models (black and red curves in Figure 3a). For the layered stiffness model, this stress maximum occurs at about 17 km depth, and the predicted zone of faulting (blue band on left of Figure 3) is very close to the 19 km depth of the Mahukona earthquake. The addition of underplating (model suite “D”) creates a low stress region at the base of the crust, deflecting the mantle stress maximum downward (black and red curves in Figure 3b). In the upper lithosphere outside of the underplate region, stresses are slightly higher compared to those of model C (Figure 3b).

4. Discussion

[13] I identify the Mahukona earthquake with the compressive stress maximum at the top of the stiffer mantle (Figure 3, blue line), consistent with the predominantly reverse mechanism for this event (Global CMT catalog, available at http://www.globalcmt.org, 2007). I attribute the initial Kiholo Bay event to the lower lithosphere extensional stress maximum, consistent with the normal component of the inferred fault mechanism and the predicted depth range of faulting for the viscoelastic/layered model “C” (Figure 3, blue band on right). A small strike slip component for Kiholo Bay (Global CMT catalog, available at http://www.globalcmt.org, 2007) may have transferred stress to the vicinity of Mahukona, thereby triggering it, especially if the former event occurred on a northward-striking fault. I

therefore interpret the two earthquakes as twins with a common birth, but expressing the opposite extremes of deformation (deep extension, shallow compression) inherent to plate flexure beneath a volcanic load.

[14] The October 15th earthquakes fall into a class of events whose focal mechanisms are consistent with a flexural stress state. A cluster of events beneath Mauna Kea with hypocenters in the range 26–32 km deep have compressional focal mechanisms, as expected for a neutral plane at depth >32 km. This is deeper than the neutral planes shown in Figure 2, but the greater load of Mauna Kea or a local increase in lithosphere thickness could account for the difference. Focal mechanisms for the 41–44 km deep 1973 Honomu event [*Wolfe et al.*, 2004] are similar to those of Kiholo Bay, with perhaps a greater strike-slip component. Kiholo Bay-type (deep) earthquakes may be more numerous than Mahukona-type (shallow), because of the greater depth range of failure for the former (Figure 3). Focal mechanisms of the largest mantle earthquakes near Kilauea often fall into a third category: low-angle thrust with the upper surface moving seaward [*Wolfe et al.*, 2003, 2004]. While such mechanisms ostensibly do not fit into the "deep extension, shallow compression" scheme of concave-upward plate flexure, the full stress tensors calculated here offer support for a flexural stress origin. The most compressive principal stress (along axis of "hourglass" symbols in Figure 2) is rotated 20–30 degrees from horizontal in the upper mantle at distances >~30 km downflank. This rotation is of sufficient magnitude and in the correct direction to produce focal mechanisms like those seen in the mantle near Kilauea. While in a strict sense plane-strain models do not account for the geometry of the young end of the Hawaiian chain, a similar stress rotation in the mantle lithosphere is observed in axisymmetric geometry [*McGovern and Solomon*, 1993].

[15] The flexural stresses calculated here also have implications for magma ascent through the lithosphere. Compressive stresses tend to inhibit magma ascent by squeezing shut vertical intrusive bodies (dikes) in the lithosphere. A strong compressive stress maximum at the top of the mantle might then trap magmas that otherwise would rise into the crust and the edifices; the stress state there would favor the emplacement of magmas in sub-horizontal sills rather than vertical dikes, thickening the volcanic pile from the bottom rather than the top (i.e., underplating). However, in a uniform-stiffness plate, the compressive trapping stress is greatest at the top (i.e., the top of the crust: black and red lines in Figure 3a), whereas beneath Hawaiian volcanoes the trapped material appears to be emplaced only near the bottom of the crust [*ten Brink and Brocher*, 1987; *Watts and ten Brink*, 1989]. The layered-stiffness model, on the other hand, predicts trapping of material beneath the crust, more consistent with the observations. I therefore suggest that stiffness-enhanced compressive stresses at the top of the mantle lithosphere are the deciding factor in underplating the crust at Hawaiian volcanoes. The underplating further depresses the crust-mantle transition (and stress maximum) by several km (Figure 3b). Thus, the correspondence of the depth of the Mahukona earthquake and the base of an underplated crust is likely not a coincidence, but rather a consequence of lithospheric control of magma ascent via the flexural stress state.

[16] The existence of a sub-crustal sill complex beneath Hawaiian volcanoes is also supported by petrological evidence. *Clague* [1988] reports that the compositions of ultramafic xenoliths from Loihi are consistent with accumulation of magmas in a storage zone (sill complex) at about 16 km below sea level, several km below the base of the crust at Loihi. Furthermore, cataclastic textures of hartzburgite xenoliths indicate a high strain rate in the storage region, consistent with the predictions of high stresses and strains in the corresponding regions of the models (Figure 2). The difference in depths to the crustal base at Loihi and northwest Hawaii (Figure 2) can be explained by the early state of flexure at the head of the Hawaiian chain (Loihi) versus the nearly complete flexural response at NW Hawaii. Nonetheless, the evidence by *Clague* [1988] demonstrates that flexural stresses may control magma ascent histories even in the earliest stages of Hawaiian edifice growth.

[17] Despite the success of the models presented here in predicting earthquake mechanisms and underplating, additional factors affect magma ascent. For example, adverse stress gradients in the mid-lithosphere (compression increasing with height, Figure 3) should inhibit magma ascent [e.g., *Rubin*, 1995; *Pritchard et al.*, 2007]. In reality, stress reductions from repeated intrusion, faulting and fluid conduits in the mantle likely mitigate such ascent barriers in the main volcanic conduits beneath the edifices [*Hieronymus and Bercovici*, 2001; *Pritchard et al.*, 2007], although the tendency of the highest-stress regions (i.e., mantle top) to provide the strongest barriers is likely to be robust. Future models that address such effects could yield a more complete understanding of the evolution of large Hawaiian edifices.

[18] **Acknowledgments.** I thank Andy Freed, Walter Kiefer, Steve Mackwell, Juli Morgan, Dan Nunes, and Allan Treiman for comments on earlier drafts, John Smith for digital topography of Hawaii, and Fenglin Niu, Paul Okubo and Cecily Wolfe for guidance on the seismic data for Hawaii. I also thank Cecily Wolfe and Jim Kauahikaua for helpful reviews. This work was supported in part by a grant from the NASA Planetary Geology and Geophysics program. LPI contribution 1343.

References

Clague, D. A. (1988), Petrology of ultramafic xenoliths from Loihi seamount, Hawaii, *J. Petrol.*, *29*, 1161–1186.

Clague, D. A., and R. P. Denlinger (1994), Role of olivine cumulates in destabilizing the flanks of Hawaiian volcanoes, *Bull. Volcanol.*, *56*, 425–434.

Eakins, B. W., J. E. Robinson, T. Kanamatsu, J. Naka, J. R. Smith, E. Takahashi, and D. Clague (2003), Hawaii's volcanoes revealed, *Geol. Invest. Ser. I-2809*, U.S. Geol. Surv., Denver, Colo.

Gramling, C. (2007), Heavy Hawaii spawns twin earthquakes, *Geotimes*, *52*(2), 36–37.

Hieronymus, C. F., and D. Bercovici (2001), Focusing of eruptions by fracture wall erosion, *Geophys. Res. Lett.*, *28*, 1823–1826.

Hill, D. P., and J. J. Zucca (1987), Geophysical constraints on the structure of Kilauea and Mauna Loa volcanoes and some implications for seismomagmatic processes, *U.S. Geol. Surv. Prof. Pap.*, *1350*, 903–917.

Karato, S.-I., M. S. Paterson, and J. D. Fitzgerald (1986), Rheology of synthetic olivine aggregates: Influence of grain size and water, *J. Geophys. Res.*, *91*, 8151–8176.

Klein, F. W., R. W. Koyanagi, J. S. Nakata, and W. R. Tanigawa (1987), The seismicity of Kilauea's magmatic system, *U.S. Geol. Surv. Prof. Pap.*, *1350*, 1019–1186.

Klügel, A., T. H. Hansteen, and K. Gallip (2005), Magma storage and underplating beneath Cumbre Vieja volcano, La Palma (Canary Islands), *Earth Planet Sci. Lett.*, *236*, 211–226.

McGovern, P. J., and S. C. Solomon (1993), State of stress, faulting, and eruption characteristics of large volcanoes on Mars, *J. Geophys. Res.*, *98*, 23,553–23,579.

McGovern, P. J., and S. C. Solomon (1998), Growth of large volcanoes on Venus: Mechanical models and implications for structural evolution, *J. Geophys. Res.*, *103*, 11,071–11,101.

Melosh, H. J., and A. Raefsky (1983), Anelastic response of the Earth to a dip-slip earthquake, *J. Geophys. Res.*, *88*, 515–526.

Nakata, J. (2007), Hawaiian Volcano Observatory seismic data, January to December 2006, *U.S. Geol. Surv. Open File Rep.*, *2007-1073*.

Pritchard, M. E., A. M. Rubin, and C. J. Wolfe (2007), Do flexural stresses explain the mantle fault zone beneath Kilauea volcano?, *Geophys. J. Int.*, *168*, 419–430, doi:10.1111/j.1365-246X.2006.03169.x.

Rubin, A. M. (1995), Propagation of magma-filled cracks, *Annu. Rev. Earth Planet. Sci.*, *23*, 287–336.

ten Brink, U. S., and T. M. Brocher (1987), Multichannel seismic evidence for a subcrustal intrusive complex under Oahu and a model for Hawaiian volcanism, *J. Geophys. Res.*, *92*, 13,687–13,707.

Turcotte, D. L., and G. Schubert (2002), *Geodynamics*, 2nd ed., Cambridge Univ. Press, Cambridge, U. K.

Watts, A. B., and U. S. ten Brink (1989), Crustal structure, flexure, and subsidence history of the Hawaiian islands, *J. Geophys. Res.*, *94*, 10,473–10,500.

Wessel, P. (1993), A re-examination of the flexural deformation beneath the Hawaiian islands, *J. Geophys. Res.*, *98*, 12,177–12,190.

Wolfe, C. J., P. G. Okubo, and P. M. Shearer (2003), Mantle fault zone beneath Kilauea volcano, Hawaii, *Science*, *300*, 478–480.

Wolfe, C. J., P. G. Okubo, G. Ekström, M. Nettles, and P. M. Shearer (2004), Characteristics of deep (≥13 km) Hawaiian earthquakes and Hawaiian earthquakes west of 155.55°W, *Geochem. Geophys. Geosyst.*, *5*, Q04006, doi:10.1029/2003GC000618.

P. J. McGovern, Lunar and Planetary Institute, USRA, 3600 Bay Area Boulevard, Houston, TX 77058, USA. (mcgovern@lpi.usra.edu)